Elucidating microscopic processes in electrochemically controlled Pb atomic-scale switches

X. Lin[1], A. Dasgupta[2], F.-Q. Xie[3], A. Groß[1], F. Evers[2], T. Schimmel[2,3]

[1] Institute of Theoretical Chemistry, University of Ulm, 89069 Ulm
[2] Institute of Nanotechnology, Karlsruhe Institut of Technology (KIT), Campus North, 76027 Karlsruhe
[3] Institute of Applied Physics and DFG-Center for Functional Nanostructure, Karlsruhe Institute of Technology (KIT), Campus South, 76131 Karlsruhe

Summary

With the single-atom transistor, a first actively switchable electronic device on the atomic scale was demonstrated. By the controlled relocation of one individual atom within an electrochemically fabricated metallic quantum point contact, an electrical current could be switched on and off. Meanwhile, we also have multi-atom switches. Changes in the atomic-scale structure within the contact area result in conductance changes of the atomic-scale contact, making conductance measurements a valuable tool to monitor atomic-scale relocation processes within the immediate contact area.

Here, we study atomic-scale relocation processes in atomic-scale lead (Pb) contacts both experimentally and with theoretical calculations and Monte-Carlo simulations. We investigate novel switching mechanisms that occur on an atomistic scale within an electrochemical environment, and develop concepts to describe them. It is shown that during the atomic-scale deposition processes diffusion plays a crucial role. For this reason as a first step barriers for self diffusion processes have been calculated using ab initio methods (density functional theory, DFT). In order to address structured surfaces more realistically, an emphasis has been put on processes near step edges. It turned out that at such edges, two-particle exchange processes are very important for the diffusion in contrast to the 'naive' direct single-particle hopping. This finding is confirmed by kinetic modelling based on Monte-Carlo simulations of the time evolution of the conductance upon closing a contact. They reveal that exchange processes involving several particles give the most important contribution for the mass-transport into the contact

volume. Such collective exchange processes are N-particle generalizations of the two-particle processes near step edges. Collective phenomena should also be important in the context of the "giant conductance fluctuations", that have been seen in the Monte Carlo simulations, but also in our experiments.

1 Introduction

The intricate interplay between the current flow and the dynamics of the atomic or molecular junction was a hot topic in molecular electronics, a present focus being on current induced forces. In our recent experiments, an atomic-scale quantum conductance switch has been realized, where the position and dynamics of a single (or few) atom(s) decides about the current flow and current switching. External control over this degree of freedom is maintained in our experiments by the electrochemical potential [1–3]. However, the details of the basic atomic switching processes are still not fully understood. Investigation of such basic atomic switching processes at or close to the tips of metal electrodes is also very important to understand electrode reconstruction in the course of single-molecule measurements in break junctions or electromigrated metallic junctions, in particular for metals that easily deform at the temperature of the experiment [4–21]. As a possible mechanism, we suggested a novel switching mechanism that is based on the collective deposition of metal atoms from the electrolyte onto the switch. Still, the exact nature of the collective process was not clarified. Here we report the results of a joint theoretical and experimental effort in order to elucidate elementary steps in the collective switching mechanism on an atomic scale and to develop concepts to describe the corresponding processes.

The fundamental elementary process occuring in the switch is the deposition of metal atoms from the electrolyte onto the metallic electrodes and the formation of a contact. The specific metal structure growing on the electrode upon metal deposition is controlled by diffusion processes. Hence a crucial part in the modeling of the atomic-scale switch is the determination of metal self-diffusion paths and the corresponding diffusion barriers. As a first step, we have therefore calculated metal diffusion barriers leading to the

formation of nanostructures using total-energy calculations based on density functional theory. As the specific metal, we have considered lead which has also been used as an electrode material in the quantum conductance switch. Note that the controlled formation of nanostructures at metal surfaces is of critical importance not only for the realization of the electrochemical quantum conductance switch, but also for several further applications at surfaces and interfaces, including catalysis [22–24], quantum [25–28] and magnetic data storage [29]. However, in spite of the fact that diffusion processes because of their importance have been studied in detail [30–32], it is fair to say that the atomic level understanding of these processes, in particular at complex, structured surfaces, is still limited. It is also important to note that the formation of the contact in the switch occurs at the electrochemical solid/liquid interface which adds further complexity to the system [33–34].

As a next step, we have performed simulations of the formation and breaking of contacts. They provide insights into the statistical nature of the motion of the electrode atoms. In particular, they show how the elementary processes – atoms moving over diffusion barriers – transform into collective many-body processes when the junction is (slowly) closed.

2 Results and Discussion

2.1 Experiment

The electrochemical deposition of atomic-scale lead contacts

For fabricating atomic-scale lead (Pb) quantum point contacts, an experimental setup was used which is illustrated in the schematic diagram of Fig. 1. Because Pb is easily oxidized at ambient conditions, the electrochemical cell is shielded within a cylindrical chamber with an observation window, three valves for gas in- and outlets, and six BNC connectors of coaxial cables for applying electrochemical potential and conductance measurement. The outlet is connected with a gas bottle full of bi-distilled water to prevent the backflow of air and thus of oxygen. The pressure is adjusted by the water level in the gas wash bottle. Before starting electrochemical deposition the

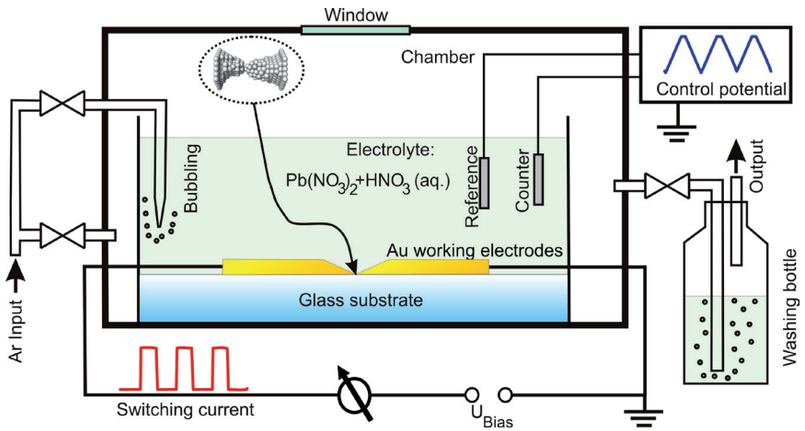

Fig. 1: Schematic diagram of the experimental setup. Pb is deposited and dissolved electrochemically in the narrow gap between two gold working electrodes (WE) on a glass substrate, and the conductance of the contact is measured simultaneously. The electrolyte consists of 1 mM $Pb(NO_3)_2$ + 0.1 M HNO_3 in bidistilled water. The experiment is performed in an oxygen-free Ar atmosphere within a protection chamber. The potentials of the WEs with respect to the lead reference electrode (RE) and the counter electrode (CE) are set by a computer-controlled potentiostat.

chamber is flowed with Argon for 6 minutes. Subsequently, the electrolyte is bubbled with Argon for approx. 2 hours to expel the remaining oxygen. After these two steps the chamber is flowed with Ar for another 3 min to take oxygen, which is expelled from the electrolyte, away from the chamber. In this way an oxygen-free environment is created for the growth of lead point contacts.

Pb atomic-scale point contacts were thus grown in an oxygen-free environment.

Two gold electrodes (thickness approx. 100 nm, width of the gap between the electrodes: approx. 50 nm) as working electrodes were covered with an insulating polymer coating except for the immediate contact area. The potentials of the working electrodes with respect to the reference and counter electrodes were set by a computer-controlled bipotentiostat. Two lead wires (0.5 mm diameter, 99.998 % purity) were used for the counter electrode and for the quasi-reference electrode. The electrolyte solution consisted of 1 mM $Pb(NO_3)_2$ + 0.1 M HNO_3 in bi-distilled water. For conductance

measurements, an additional voltage of 12.9 mV was applied between the two gold electrodes. The variation of the electrochemical potential difference between the reference electrode and the gold working electrodes was performed by varying the control potential of the reference electrode relative to the ground potential.

To fabricate an initial Pb contact in the gap between the two gold electrodes, we apply a potential of 10–20 mV to the reference electrode. While Pb islands are deposited in the junction we monitor the conductance between the two electrodes until a contact of preset conductance value is formed. Such a contact typically survives in repeated opening/closing cycles for many days.

Experimental results

The experiments obtained on switching events within metallic quantum point contacts provide the basis and the motivation for the subsequent theoretical studies, which aim at describing the underlying dynamic processes on the metallic surface and within the immediate contact area and at describing the basic mechanisms leading to these bistabilities.

Spontaneous switching between two different conductance values is, under certain conditions, encountered in metallic atomic-scale point contact experiments. Earlier experiments studying the electrochemical contact formation and switching of silver and lead atomic-scale point contacts are given in Ref. [35–38]. Figure 2 shows two kinds of bistable switching events in the Pb atomic-scale point contacts. The blue graphs display the variation of electrochemical potential applied to the quasi-reference electrode, while the red curves illustrate the conductance change following the variation of the electrochemical potential. In this experiment, the computer-controlled ramping rate of electrochemical potential is 50 mV/s. In Fig. 2a the conductance fluctuates between 0.3 G_0 and 0.9 G_0. The potential is varied between –27 mV and 12 mV. Due to computer control, the potential follows the change of the conductance with a preset threshold of the conductance at 0.4 G_0. When the conductance surpasses 0.4 G_0, the computer-controlled electrochemical potential is lowered again, with a lower threshold of –27 mV. When the conductance is measured less than 0.4 G_0, the controlled potential goes

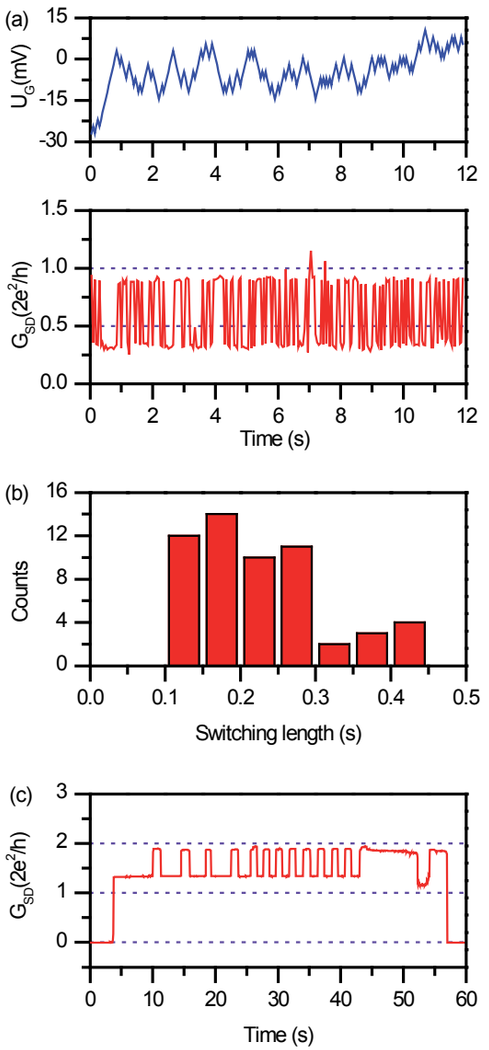

Fig. 2: Bistable swtiching in atomic-scale Pb point contacts. Diagram (a) displays an occasionally observed random switching phenomenon. Diagram (b) gives the statistics of the time between subsequent switching events, derived fron the data presented in (a). Fig. (c) shows an example of spontaneous, rather regular bistable switching between two well-defined conductance levels.

up, with an upper threshold of 12 mV. A minor changes of the electrochemical potential result in a dramatic jump of the conductance. It is observed that now, the conductance switches randomly between two levels. This kind of phenomenon is observed in our experiments with Pb atomic-scale point contacts occasionally. Fig. 2b shows the statistics of the switching length presented in Fig. 2a. Typical switching times between conductance changes are between 0.1 s and 0.3 s. Fig. 2c gives an example of spontaneous, rather regular bistable switching between two well-defined conductance levels, a behavior which is only occasionally observed. The conductance in this case switches between approx. 1.3 G_0 and 1.9 G_0.

2.2 Theoretical Methods

The first-principles total energy calculations were performed using a periodic DFT programme, the Vienna ab initio simulation (VASP) package [34]. To describe the exchange-correlation effects, we used the generalized gradient approximation (GGA) employing the Perdew, Burke and Ernzerhof (PBE) exchange-correlation functional [39]. The electronic one-particle states have be expanded in plane-waves up to an cutoff energy of 400 eV.

Within the supercell approach, the Pb electrodes were modeled by slabs of finite thickness separated by a vacuum region of 20 Å, which is sufficient to neglect the interactions between the periodic slabs. Five layers have been used to describe the Pb(100) and Pb(111) surfaces. For the stepped surfaces, 10 layers for Pb(311), 15 layers for Pb(211) / Pb(511) and 20 layers for Pb(711) surfaces have been used. The optimized position were relaxed until the residual forces were smaller than 0.01 eV/Å using a 3 x 3 supercell for Pb(111)/ Pb(100) and 1 x 3 supercell for stepped surfaces. A k-point sampling of 5 x 5 x 1 k-point were used to perform the integration over the first Brillouin zone. The convergence of the results with respect to these parameters has been carefully checked. To determine the diffusion paths in the exchange mechanism, the nudged elastic band method (NEB) was employed [40], which is an automatic search routine for finding the energy minimum path between specified initial and final state.

In order to understand the qualitative phenomena related to the closure of a junction, it is both sufficient and most efficient to employ Metropolis

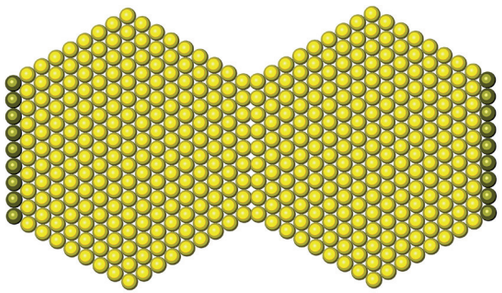

Fig. 3: Typical initial configuration employed for Monte-Carlo-simulations of contact-breaking/bistability dynamics. In our simulations, the positions of the left and right boundary atoms (dark) is frozen while all other atoms move freely inside a fixed wall bounding box.

Monte-Carlo simulations in canonical ensembles [41], using semi-empirical interaction potentials; hence, we simulated the junction dynamics with a tight-binding second-moment approximation model (TBSMA) also known as the Gupta-potentials [42]. Moreover, the collective phenomena are not specific to three spatial dimensions. They appear already in film geometries, as we see, and hence we concentrate on mono-atomic layers in our simulations, see Fig. 3.

The contact formation and breaking dynamics is simulated, starting from an initial configuration, which may or may not be stressed by positioning fixed bounding layers. The structures are then relaxed/equilibrated for 10000 steps per atom, to avoid any artifacts before collection of statistics begins. For breaking, the distance of the left and right boundary layers (Fig. 3) is fixed. This distance controls the equilibrium conductance and will be varied to open and close the junction. To observe the time evolution of contact closure an initial situation will be chosen, where the contact layer (middle row in Fig. 3, 9 atoms) consists of a single atom, only. One may think about it as an atom that has been quenched when the electrodes have approached each other in the experimental control cycle. For contact opening, we increase the distance between the boundary layers. The numerical protocol foresees an adiabatically slowly process, so that at every distance for most of the observation time the contact is (nearly) equilibrated.

For numerical efficiency we used a potential truncation scheme using a mixed Verlet list automatically updated by a Cell list [41]. A large cutoff (~7 x nearest neighbor distance) was used to avoid any possible truncation errors. The TBSMA used in our simulations is a true many-body potential which for an N-atom system requires N^2 loops for evaluation of energy; this

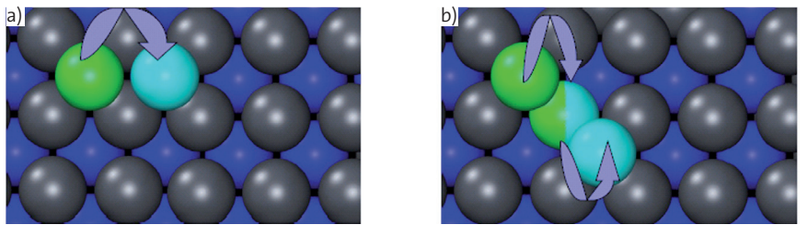

Fig. 4: Illustration of a) hopping diffusion, b) exchange diffusion on a (100) surface.

in conjunction with the fact that we define a Monte Carlo time step as 10 x N computational steps makes the simulations roughly have an approximate computational cost N^3. Our implementation of the truncation scheme along with a look up table for energy calculations brings down the computational time by a factor of 10 without introducing any untoward artifacts. A typical simulation usually involves 10^5 MC steps for equilibration followed by 10^6 MC steps for collection of statistics.

2.3 Theoretical Results and Discussion

Metal diffusion studied by DFT calculations

After metal deposition on a surface, the resulting surface structure is determined by the fact whether the deposited atoms propagate further on via diffusion and how facile the diffusion is. Generally speaking, there are two kinds of diffusion mechanisms, the hopping mechanism and the exchange mechanism which are illustrated in Fig. 4a and b, respectively. The hopping mechanism is considered as the usual mode of the diffusion by which atoms move between the adjacent equilibrium sites. It is mainly operative on closed packed metal surfaces. In the exchange mechanism, the adatom displaces a surface atom which then becomes the adatom. It has typically been observed on (100) surfaces such as Pt(100) [43] or Ir(100) [44]. Whereas in the hopping mechanism the transition state corresponds to the hopping atom in a two-fold coordination, in the exchange mechanism there are two atoms in a three-fold coordination at the transition state. Hence the exchange mechanism is operative at metal surfaces that favor a three-fold coordination.

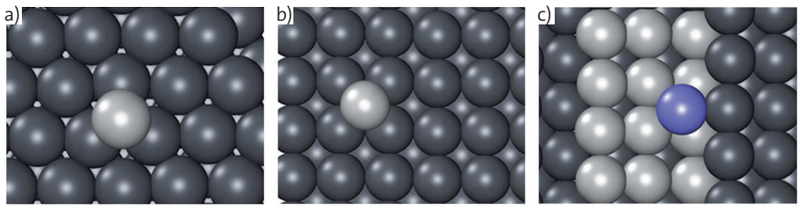

Fig. 5: Optimized adsorption position of a Pb adatom on a) Pb(111) , b) Pb(100), c) Pb(511).

As the first step to address the diffusion paths, we determined the optimum adsorption position of a Pb adatom on flat and stepped Pb surfaces (see Fig. 5). For Pb(111) and Pb(100) we find, as expected, that the equilibrium geometry are the threefold hollow site (Fig. 5a) and the fourfold hollow site (Fig. 5b), respectively. On Pb(111), the adatom adsorption height is 2.23 Å, the distance to the nearest neighbors is 3.13 Å which is 12 % shorter than the interatomic distance in the bulk. As for Pb(100), the adatom adsorption height is 1.96 Å, and the distance to the nearest neighbors is 3.21 Å which is 9 % shorter than the interatomic distance in the bulk. These trends are typical for adsorbed metal atoms and can be explained in terms of the correlation between bond strength and coordination [45,46].

On Pb(511), the adatom prefers to adsorb at the lower side of the step edge in direct contact with one step atom in an bridge-like site with respect to the atoms of the lower terrace. (Fig.5c). Because of this bridge-like configuration, the adsorption height is 3.27 Å with respect to the lower terrace, and the distance between the adatom and the step edge is 3.39 Å. As all other considered (n11) stepped surfaces with odd n have rather similar properties, we focus in the discussion on the (511) surfaces and just report the results for the other stepped surfaces.

Table 1 shows the diffusion barriers on the flat Pb(100) and Pb(111) surfaces. On the Pb(111) surface, we obtained an energy barrier of only 0.01 eV for the hopping mechanism and 0.11 eV for the exchange mechanism which is about 10 times larger than for the hopping process. But interestingly enough, on Pb(100) the diffusion barrier of the exchange mechanism is 0.47 eV which is 0.17 eV lower than for hopping indicating that the exchange diffusion is the favorable mechanism on Pb(100).

Tab. 1: Diffusion barriers for Pb adatoms on flat Pb surfaces.

Surface	Hopping (eV)	Exchange (eV)
Pb(111)	0.01	0.11
Pb(100)	0.64	0.47

The diffusion constant is given by the Arrhenius formular: $D = D_0 \exp(-E_d/k_B T)$, where E_d is the diffusion barrier. Many studies show that the prefactor D_0 for exchange diffusion is usually 10–15 times larger than the one for hopping diffusion [47, 48], hence the exchange is obviously favored for Pb(100), which is similar for Au(100). Note that the two atoms exchanging each other are rather close to each other at the transition state, only about 3.15 Å. Furthermore, the dimer is only 1.44 Å above the surface, so that the two atoms can be described as practically being fivefold coordinated. Hence it is obviously this high coordination that makes the exchange diffusion on Pb(100) more favorable than the hopping diffusion.

At stepped surface, the diffusion paths are much more complex. First of all, one has to distinguish diffusion along the step edge from diffusion perpendicular to the step edge, i.e. across the step edge. For the exchange mechanism along and across the step edge, there are several possibilities. All the atoms in light grey and white in Fig. 6 may be partners in the exchange diffusion of the adatom along and perpendicular to the step.

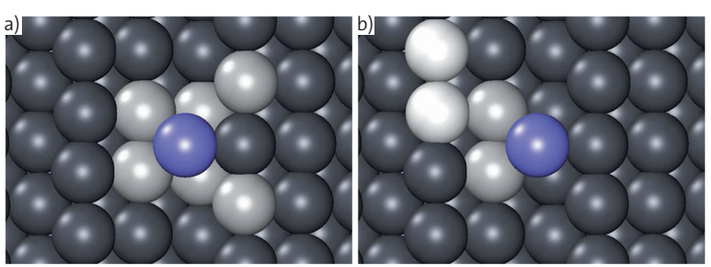

Fig. 6: Surface atoms (in light grey) which might exchange with the adatom (in blue). a) diffusion along the step edge. b) diffusion perpendicular to the step edge. The atoms colored in light grey may be involved in the diffusion across the terrace while the atoms colored in white may be part of the exchange mechanism across the step.

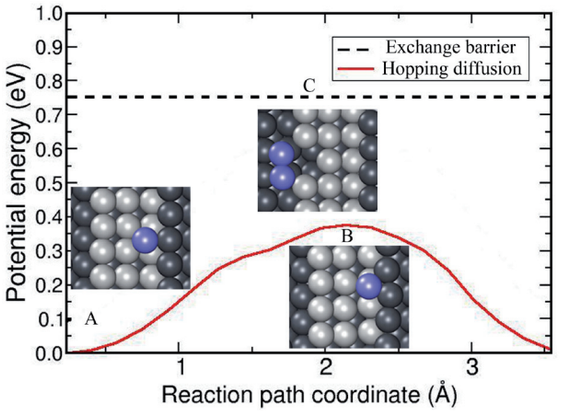

Fig. 7: Minimum energy path of the hopping mechanism for the diffusion along the step at Pb(511). Insets A and B illustrate the initial and transition state of the hopping mechanism. The barrier for the exchange mechanism is indicated by the dashed line, its configuration is shown in inset C.

The minimum energy diffusion paths on Pb(511) are illustrated in Figs. 7 and 8. As shown in Fig. 7, for the difusion along the step edge, the barrier of hopping diffusion is 0.39 eV lower than for the exchange mechanism. The hopping process occurs close to the step edge (inset B of Fig. 7) and involves some relaxation of the step edge atoms. This relatively low barrier can be explained by the fact that the coordination of the hopping atom does not change significantly along the diffusion path. In the exchange mechanism, on the other hand, the step edge atom has to detach almost entirely from the lower terrace making this mechanism rather unfavorable. The mechanism is quite similar to the diffusion process on Al(110) in the so- called in-channel diffusion [47].

For the diffusion across the terrace perpendicular to the step edge, the exchange mechanism is most favorable, as Fig. 8 shows. The diffusion in the middle of the terrace is almost the same as the diffusion process on the flat Pb(100) surface with a very similar energy barrier. Across the step edge, the energy barrier for the exchange process is much lower than for the hopping mechanism. The high barrier in the hopping mechanism of 0.93 eV is caused by the low coordination at the transition state, whereas in the exchange process (inset A of Fig. 8.), the coordination number of the adatom is only

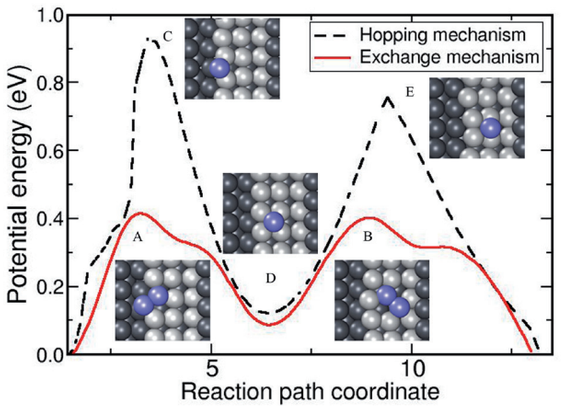

Fig. 8: Minimum energy path of the hopping and exchange mechanisms on Pb(511) across the step edge. Insets A and B show intermediate states of the exchange diffusion whereas insets C and E illustrate intermediate states in the hopping diffusion. Inset D shows the metastable intermediate on the terrace.

reduced from five at the initial state at the lower edge of the step to four at the transition state leading to a relatively low diffusion barrier.

All calculated diffusion barriers at the considered stepped Pb surfaces, Pb(311), Pb(511) and Pb(711), are listed in Table 2. As already mentioned above, all of the stepped surfaces have rather similar properties, as far as diffusion is concerned. Whereas along the steps the hopping mechanism is favored, across the steps the diffusion occurs in a exchange mechanism.

So far, we have entirely neglected that the formation of the contact in the switch occurs at the electrochemical solid/liquid interface. Neglecting the

Tab. 2: The diffusion barriers at stepped Pb surfaces.

Surface	Hopping (eV)	Exchange (eV)
Pb(311)par	0.33	0.36
Pb(311)per	0.95	0.57
Pb(511)par	0.36	0.75
Pb(511)per	0.93	0.41
Pb(711)par	0.37	0.73
Pb(711)per	0.97	0.56

influence of the aqueous electrolyte can be justified by the fact that water is relatively weakly interacting with flat metal electrodes and hardly influences the electronic structure [33]. Still, water layers at metal surfaces can be strongly polarized [33, 49] and thus induce field effects that might modify the surface structure [50], in particular at stepped surfaces. Indeed, recently a large reduction of the Helmholtz capacitance or inner-layer capacitance on stepped gold and silver surfaces has been observed [51] which indicates strong polarization effects at stepped metal electrodes at the electrochemical electrode/electrolyte interface. In order to elucidate the structure of water on stepped surfaces, the vibrational spectra of a water layer on Au(100) and Au(511) were measured in detail using electron energy loss spectroscopy (EELS) [52]. Based on the EELS spectra, a structural model for the water layer on Au(511) was proposed [52]. This structural model was confirmed in ab initio molecular dynamics simulations based on periodic DFT calculations [53].

Furthermore, a strong interaction of the water molecules with the step edge atoms was found which is accompanied by a strong polarization of these water molecules. This might explain the observed large reduction of the Helmholtz capacitance on stepped surfaces [53]. It still remains to be seen which effect this strong polarization has on the diffusion properties at the steps. This is the subject of ongoing research.

Monte Carlo simulation of contact formation, breaking, bistability

In the preceding section we have identified the role of two-particle exchange processes for the diffusion dynamics across step edges. We will now report observations from our Monte Carlo studies. They suggest that two-particle exchange should be viewed as the simplest representative of a class of processes involving N particles and M vacancies (or holes); in the example we have N=2, M=1. The time evolution of these processes is such that all M vacancies are filled with particles thereby creating M new vacancies at other sites. In a lose way of speaking, one could say that M particles (vacancies) have been moved from old positions into new positions. (Processes with M=0 are "ring exchange" processes, i.e. cyclic permutations. Due to the fact that atoms are not distinguishable one from another, these processes are not accompanied with density fluctuations. Therefore, they can be ignored for thermodynamic considerations.)

As our previous study shows, on flat surfaces only processes with N,M=1 are important, because motion of N-particles, in general, involves the breaking of ~N bonds and therefore very high activation barriers. The situation changes, however, in the presence of transport barriers. Again the step-edge is only the simplest example. In inhomogenous situations, internal vacancies can exist that are very difficult to reach, or not at all, for an adsorbate particle via a path, that never leaves the vacuum interface. In such a situation (N,M)-processes can become relevant and may provide the only available route for a particle to fill the vacancy (or equivalently, for the vacancy to merge with the vacuum).

Contact formation: (N,1) exchange processes

Fig. 9 shows three snapshots showing how a contact forms after the electrodes have quenched a single atom, see initial state Fig. 9A. The contact atom is surrounded by vacancies to the left and to the right. In Fig. 9A a single vacancy on each side is shown; for broader junctions it can be many more. These vacancies cannot be filled easily by surface diffusion of the adsorbate atoms (blue), since the associated barrier height for the process is high. It is true, that also a given (N,1) exchange process is associated by a large barrier height. However, due to the large number of possible exchange paths, these processes can become compatible and in fact dominate in the situation shown in Fig. 9. This is evident, from Figs. 9B and 9C that indicate the typical exchange processes that have been responsible for filling the junction in our MC-simulations.

A general quantitative analysis that could illuminate under what precise conditions (N,M) exchange processes with N>1 start to dominate over the simple hopping is challenging. On the one hand, it should comprise an estimate of the height of a multi-particle tunneling barrier that is the characteristic feature of the collective hopping phenomena that we describe here. On the other hand, also required is an enumeration of all those (N,M)-reorderings that share the starting and end-configurations. Summarizing in a symbolic notation, we have for the thermodynamic weight of a given (N,1)-exchange process $A_1(N) \sim e^{W(N)}e^{-P(N)}$ with an entropic term $W(N) \approx w(N)N$ and an hopping barrier for the N-particle process $P(N) \approx v(T)N/T$. Microscopic

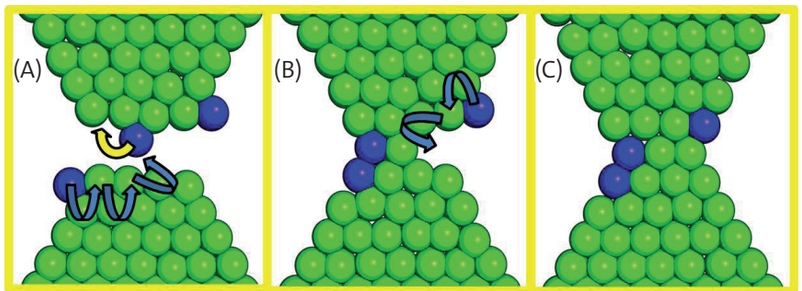

Fig. 9: Three snapshots (A), (B), (C) of a 3-atom junction towards closure: Yellow arrows denote (1, 1) processes while the blue arrow denotes (N, 1), N being number of arrows, whereas the green/blue balls denotes the initial interface-adatoms. The arrows indicate where the atoms would end up in the next frame as a result of these processes. E.g., in going from (A) to (B) we encounter a (1,1) hopping of an adatom and a (3,1) exchange process.

details of the contact and path geometry enter the prefactors and coefficients, that have been suppressed here. The most probable path follows from a saddle point analysis of the effective action S(N) = W(N)-P(N).

A more precise theory of N-particle hopping dynamics would proceed via a path integral formulation in the N-particle configuration space. The most likely path corresponds to the saddle point solution of the effective action S(N). In the following we refrain from the attempt to provide such an analytical investigation. We extract from our formulas only the information that the probability for an N-particle process to close the junction varies like $e^{(w(N)-v(T)/T)N}$. Hence, the waiting time for observing such reorderings in our MC-simulation grows exponentially large, once the temperature has fallen below a lower limit T < v(T)/w(N).

Contact breaking and bistability – rare events

We now provide numerical evidence, that illustrates the importance of exponentially long time scales also when a contact is being broken. Fig. 10 shows contacts at three different stress levels (distances of the boundary layers). For comparatively low stresses Fig. 10a, 0.9 %, spontaneous conductance switching between 7–9 G_0 (G_0= $2e^2/h$) is observed. Only slightly increasing

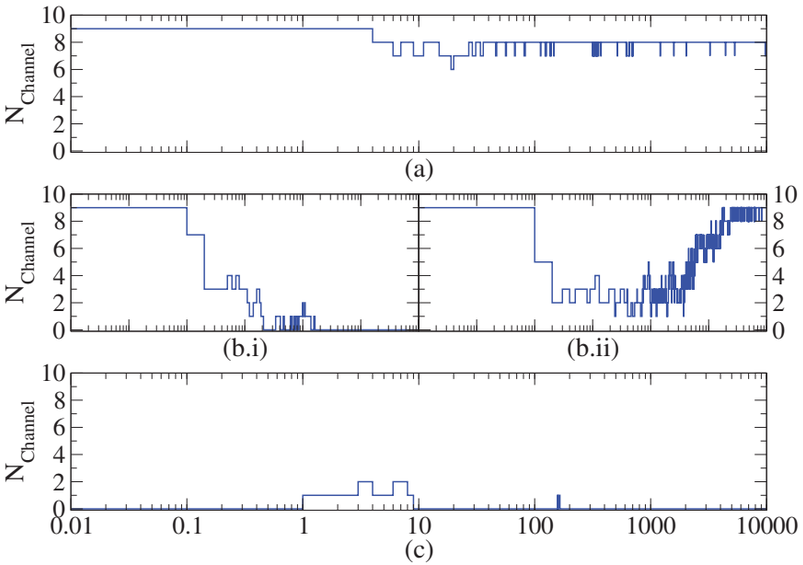

Fig. 10: Evolution of the number of open channels with increasing (Monte-Carlo) time for a 9- atom junction in a 464 atomic system, running at 464 K, under strain: (a) at 0.9 %, (b) at 1.2 % and (c) at 1.5 %. To illustrate the statistical nature of the time evolution, for strain value 1.2 % two traces are shown in inset (b) that only differ in the inherent randomness of Monte Carlo dynamics.

the stress further, 1.2 %, exhibits a bistability, Fig. 10b.ii. The conductance first decreases and depending on the detailed microscopic initial condition the junction can even break. However, the junction can also recover and even close again. One expects to observe many of such giant conductance fluctuations with observation times, exponentially much longer than available in standard numerical simulations. That indeed even a junction after going down to zero conductance, can exhibit fluctuating currents is illustrated in the bottom panel of Fig. 10.

The spontaneous fluctuation that we observe in Fig. 10.b.ii. exhibits a closing phase at t>1000. This process is a close relative, in principle, of the closure of the junction described before. In particular, one expects that also here N-particle exchange processes are going to play an important role.

Comparison to experiment and outlook

Spontaneous switching between two different conductance values is, under certain conditions, also a common encounter in the experiments presented above, see e. g. Fig. 2 a, c. We take the second-time-scale seen there as an illustration of the rare-event character of the salient microscopic processes. We believe that the underlying physics is qualitatively similar to what we also see in the simulations (e.g., in Fig. 10): at longest observation times. As a next step a more detailed statistical comparison between switching events in experiment and model calculations would be desirable. With our work we have been able to lay grounds for such a study, because the phase space corner has been identified, where spontaneous switching can be found in the model phase space. At this point in time, a further comparison is impaired, however, due to the enormous demand on computer power associated with the long time series needed to obtain good statistics. We have to relegate this interesting task to future research.

3 Conclusion

In a combination of first-principles electronic structure calculations, simulations and experiments we have addressed elementary processes that may be relevant in the collective switching mechanism occuring in the atomic-scale quantum conductance switch. The DFT calculations revealed that diffusion processes across the step edges of nanostructured surfaces are facilitated through the exchange mechanism. Such exchange processes and in fact more generalized versions of them have also been observed in Monte-Carlo simulations. It was seen how they can play an important role in the closing dynamics of junctions with large conductances. Moreover, parameter regimes have been identified, where the MC simulations show spontaneous switching with giant conductance fluctuations due to such collective reorderings of many particles. Similar processes also were experimentally observed in Pb atomic-scale point contacts.

Acknowledgements

This work was supported by the Baden-Württemberg Foundation within the Network of Excellence “Functional Nanostructures”, as well as the Deutsche Forschungsgemeinschaft within the Center for Functional Nanostructures (CFN), and the Volkswagen-Stiftung. We thank I. Kondov (Steinbuch Computing Center at the Karlsruhe Institute of Technology) as well as the Juelich Supercomputer Center (Project HKA12) for computational support. Additional computational resources were provided by the bwGRiD project of the State of Baden-Württemberg / Germany and by a computer cluster financed through the stimulus programme “Electrochemistry for Electromobility” of the German Ministry of Education and Science (BMBF).

References

[1] F.-Q. Xie, L. Nittler, Ch. Obermair, and T. Schimmel. Phys. Rev. Lett. **93**, 128303, 2004

[2] F.-Q. Xie, R. Maul, Ch. Obermair, E. B. Starikov, W. Wenzel, G. Schön, and T. Schimmel. Nano Letters **8**, 4493–4497, 2008

[3] Ch. Obermair, F.-Q. Xie, and T. Schimmel. Europhys. News. EPN**41**/4, 25–28, 2010

[4] F. May, M. R. Wegewijs, and W. Hofstetter. Beilstein J. Nanotechnol. **2**, 693–698, 2011

[5] C. A. Martin, D. Ding, J. K. Sørensen, T. Bjørnholm, J. M. van Ruitenbeek, and H. S. J. van der Zant. J. Am. Chem. Soc. **130**, 13198–13199, 2008

[6] W.-J. Hong, H. Valkenier, G. Mészáros, D. Zsolt Manrique, A. Mishchenko, A. Putz, P. Moreno Garcia, C. J. Lambert, J. C. Hummelen, and T. Wandlowski. Beilstein J. Nanotechnol. **2**, 699–713, 2011

[7] E. Lörtscher, H. B. Weber, and H. Riel. Phys. Rev. Lett. **98**, 176807, 2007

[8] T. N. Todorov, D. Dundas, A. T. Paxton, and A. P. Horsfield. Beilstein J. Nanotechnol. **2**, 727–733, 2011

[9] T. Shiota, A. I. Mares, A. M. C. Valkering, T. H. Oosterkamp, and J. M. van Ruitenbeek. Phys. Rev. B **77**, 125411, 2008

[10] M. L. Perrin, C. A. Martin, F. Prins, A. J. Shaikh, R. Eelkema, J. H. van Esch, J. M. van Ruitenbeek, H. S. J. van der Zant, and D. Dulić. Beilstein J. Nanotechnol. **2**, 714–719, 2011

[11] S. Y. Quek, M. Kamenetska, M. L. Steigerwald, H. J. Choi, S. G. Louie, M. S. Hybertsen, J. B. Neaton, and L. Venkataraman. Nature Nanotech. **4**, 230–234, 2009

[12] M. Strange and K. S. Thygesen. Beilstein J. Nanotechnol. **2**, 746–754, 2011

[13] M. Kamenetska, M. Koentopp, A. C. Whalley, Y. S. Park, M. L. Steigerwald, C. Nuckolls, M. S. Hybertsen, and L. Venkataraman. Phys. Rev. Lett. **102**, 126803, 2009

[14] S. Nakashima, Y. Takahashi, and M. Kiguchi. Beilstein J. Nanotechnol. **2**, 755–759, 2011

[15] H. Song, Y. Kim, J. Ku, Y. H. Jang, H. Jeong, and T. Lee. Appl. Phys. Lett. **94**, 103110, 2009

[16] J.-T. Lü, T. Gunst, P. Hedegård, and M. Brandbyge. Beilstein J. Nanotechnol. **2**, 814–823, 2011

[17] M. Häfner, J. K. Viljas, and J. C. Cuevas. Phys. Rev. B **79**, 140410, 2009

[18] G. C. Solomon, J. P. Bergfield, C. A. Stafford, and M. A. Ratner. Beilstein J. Nanotechnol. **2**, 862–871, 2011

[19] J. Edwin Hobi, A. Fazzio, and A. J. R. da Silva. Phys. Rev. Lett. **100**, 056104, 2008

[20] J. P. Bergfield, J. D. Barr, and C. A. Stafford. Beilstein J. Nanotechnol. **3**, 40–51, 2012

[21] N. Bode, S. V. Kusminsky, R. Egger, and F. von Oppen. Beilstein J. Nanotechnol. **3**, 144–162, 2012

[22] F. Buatier de Mongeot, A. Toma, A. Molle, S. Lizzit, L. Petaccia, and A. Baraldi. Nanoscale Res. Lett. **2**, 251–264, 2007

[23] T. E. Madey, W. Chen, H. Wang, P. Kaghazchi, and T. Jacob. Chem. Soc. Rev. **37**, 2310–2327, 2008

[24] A. Groß. J. Comput. Theor. Nanosci. **5**, 894–899, 2008

[25] D. Loss and D. P. DiVincenzo. Phys. Rev. A **57**, 120–126, 1998

[26] M. Nomura, N. Kumagai, S. Iwamoto, Y. Ota, and Y. Arakawa. Nat. Phys. **6**, 279–283, 2010

[27] H. Oka, P. A. Ignatiev, S. Wedekind, G. Rodary, L. Niebergall, V. Stepanyuk, D. Sander, and J. Kirschner. Science **327**, 843–846, 2010

[28] L. Wang, A. Rastelli, S. Kiravittaya, M. Benyoucef, and O. G. Schmidt. Adv. Mater. **21**, 2601–2618, 2009

[29] J. I. Martin, J. Nogues, K. Liu, J. L. Vicent, and I. K. Schuller. J. Magn. Mater. **256**, 449–501, 2003

[30] T.-Y. Fu and T. T. Tsong. Surf. Sci. **454**, 571–574, 2000

[31] T.-Y. Fu, L.-C. Cheng, Y.-J. Hwang, and T. T. Tsong. Surf. Sci. **507**, 103–107, 2002

[32] P. J. Feibelman. Phys. Rev. Lett. **65**, 729–732, 1990

[33] S. Schnur and A. Groß. New J. Phys. **11**, 125003, 2009

[34] G. Kresse and J. Furthmüller. Phys. Rev. B **54**, 11169–11186, 1996

[35] R. Maul, F.-Q. Xie, Ch. Obermair, G. Schön, T. Schimmel, and W. Wenzel. Appl. Phys. Lett. **100**, 203511, 2012

[36] F.-Q. Xie, F. Hüser, F. Pauly, Ch. Obermair, G. Schön, and T. Schimmel. Phys. Rev. B **82**, 075417, 2010

[37] Ch. Obermair, H. Kuhn, and T. Schimmel. Beilstein J. Nanotechnol. **2**, 740–745, 2011

[38] F.-Q. Xie, R. Maul, Ch. Obermair, W. Wenzel, G. Schön, and T. Schimmel. Adv. Mater. **22**, 2033–2036, 2010

[39] J. P. Perdew, K. Burke, and M. Ernzerhof. Phys. Rev. Lett. **77**, 3865–3868, 1996

[40] G. Henkelman and H. Jonsson. J. Chem. Phys. **113**, 9978–9985, 2000

[41] D. Frenkel and B. Smit. Understanding Molecular Simulation: From Algorithms to Applications, Academic Press, San Diego, 1996.

[42] F. Cleri and V. Rosato. Phys. Rev. B **48**, 22–33, 1993

[43] G. L. Kellogg and P. J. Feibelman. Phys. Rev. Lett. **64**, 3143–3146, 1990

[44] C. Chen and T. T. Tsong. Phys. Rev. Lett. **64**, 3147–3150, 1990

[45] B. D. Yu and M. Scheffler. Phys. Rev. B **56**, R15569, 1997

[46] L. J. Pauling. J. Am. Chem. Soc. **53**, 1367–1400, 1931

[47] R. Stumpf and M. Scheffler. Phys. Rev. B **53**, 4958–4973, 1996

[48] K. C. Pandey. Phys. Rev. Lett. **57**, 2287–2290, 1986

[49] J.-S. Filhol and M.-L. Bocquet. Chem. Phys. Lett. **438**, 203–207, 2007

[50] A. Y. Lozovoi, and A. Alavi. Phys. Rev. B **86**, 245416, 2003

[51] G. Beltramo, M. Giesen, and H. Ibach. Electrochim. Acta **54**, 4305–4311, 2009

[52] H. Ibach. Surf. Sci. **604**, 377–385, 2010

[53] X.-H. Lin, and A. Groß. Surf. Sci. **606**, 886–891, 2012